

EUROPEAN SOUTHERN
OBSERVATORY



BULLETIN NO. 8

The Governments of Belgium, the Federal Republic of Germany, France, the Netherlands, and Sweden have signed a Convention¹⁾ concerning the erection of a powerful astronomical observatory on October 5, 1962.

By this Convention a European organization for astronomical research in the Southern Hemisphere is created. Denmark became a member of the organization on June 1, 1967. The purpose of this organization is the construction, equipment, and operation of an astronomical observatory situated in the Southern Hemisphere. The initial program comprises the following subjects:

1. a 1.00 m photoelectric telescope,
2. a 1.50 m spectrographic telescope,
3. a 1.00 m Schmidt telescope,
4. a 3.60 m telescope,
5. auxiliary equipment necessary to carry out research programs,
6. the buildings for administration, laboratories, workshops, and accommodation of personnel.

The site of the observatory is in the middle between the Pacific coast and the high chain of the Andes, 600 km north of Santiago de Chile, on La Silla, at an altitude of 2400 m.

The geographical coordinates of the main summit of La Silla are

$$\begin{aligned}\lambda &= + 70^\circ 43' 46.''50 \\ \varphi &= - 29^\circ 15' 25.''80\end{aligned}$$

They were determined by the Instituto Geográfico Militar of Santiago/Chile.

¹⁾ The ESO Management will on request readily provide for copies of the Paris Convention of 5 October 1962.

Organisation Européenne pour des Recherches Astronomiques
dans l'Hémisphère Austral

EUROPEAN SOUTHERN
OBSERVATORY



BULLETIN NO. 8

June 1971

Edited by European Southern Observatory, Office of the Director
Bergedorfer Straße 131, 205 Hamburg 80, Fed. Rep. of Germany

ESO BULLETIN NO. 8

CONTENTS

B. E. Westerlund: Meteorological observations on La Silla in 1969	5
G. Lemaître: Sur la flexion du grand miroir de 3,60 m de European Southern Observatory	21
Anne B. Underhill: Observing Programs for Early Type Stars with Extended Atmospheres	33

METEOROLOGICAL OBSERVATIONS ON LA SILLA IN 1969

B. E. Westerlund

Introduction

The observations concern cloudiness, wind velocity, wind direction, temperature, and humidity as in previous years. They have been obtained at point S (between the 1.52 m telescope building and the 1 m telescope building) and at point T (second highest top, 2400 m). Mr. F. Middelburg has supervised the observations and compiled the tables.

Clouds

The observations cover all 365 nights of the year. In Table 1 the percentages of photometric nights are given for each month. The observations of 1965, 1966, 1967 and 1968 are given for comparison. All nights having six or more hours of uninterrupted clear sky are defined as „photometric nights“. The last column gives the mean values for 1966—1969. The values for 1965 have not been included as they are based on less complete observations than those of the other years.

Table 1: Percentage of photometric nights

Month	1965	1966	1967	1968	1969	Mean of 1966—1969
January	—	100	94	71	58	81
February	73	96	100	62	82	85
March	79	94	90	81	71	84
April	33	57	73	70	50	63
May	15	58	35	55	39	47
June	6	47	67	38	20	43
July	9	36	52	42	35	41
August	25	64	39	58	52	53
September	63	70	52	37	53	53
October	63	64	58	49	45	54
November	65	50	57	80	67	64
December	77	94	71	90	84	85

Out of the total of 3681 hours during which observations might have been made, 1996 hours were totally clear. This compares unfavourably with 2481 hours in 1966, 2412 hours in 1967, and 2197 hours in 1968.

The number of photometric clear nights in 1969 was 199. This is less than in previous years: 252 in 1966, 239 in 1967, and 223 in 1968.

In Fig. 1 the percentage of clear nights, indicated on the vertical axis, is plotted against the month of the year for 1969 and for the mean of 1966—1969.

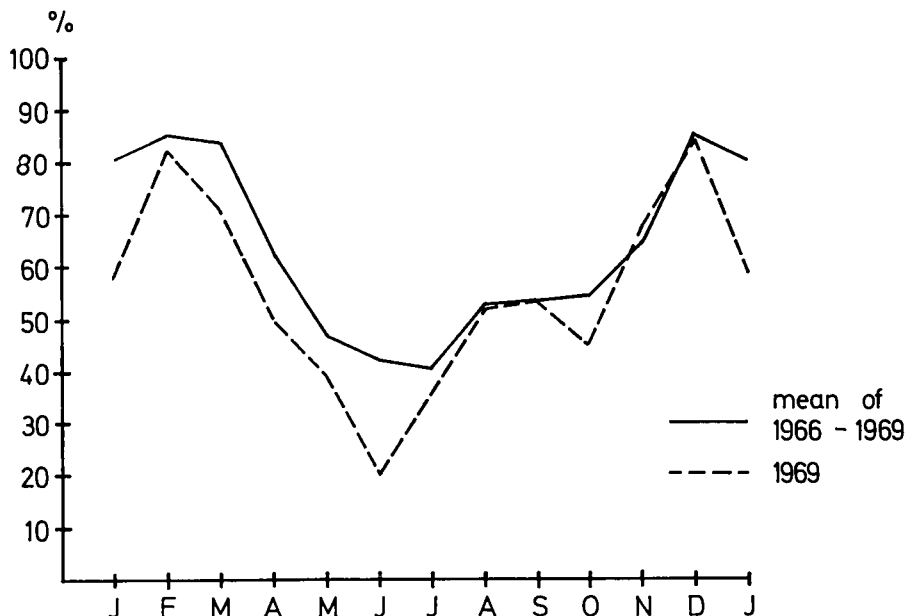


Fig. 1 : Photometric nights.

Maximum wind velocities during each month

In Table 2 the maximum wind velocities in m/s are given for each month as recorded at sites S and T. The maximum wind velocities are taken from all observations, regardless of cloudiness.

Table 2: Maximum wind velocity in m/s at S and T

1969	S	T	1969	S	T
January	15	—	July	18	19
February	7	9	August	20	22
March	19	22	September	18	20
April	20	22	October	33	35
May	22	23	November	17	18
June	25	26	December	10	12

Meteorology 1969 on La Silla

In Fig. 2 the maximum wind velocity at S is plotted against the month of the year for 1966 through 1969. On the vertical axis the wind velocity is given in m/s, on the horizontal axis the months of the year are given.

1969 gave the highest wind velocity, 33 m/s, recorded on La Silla until now.

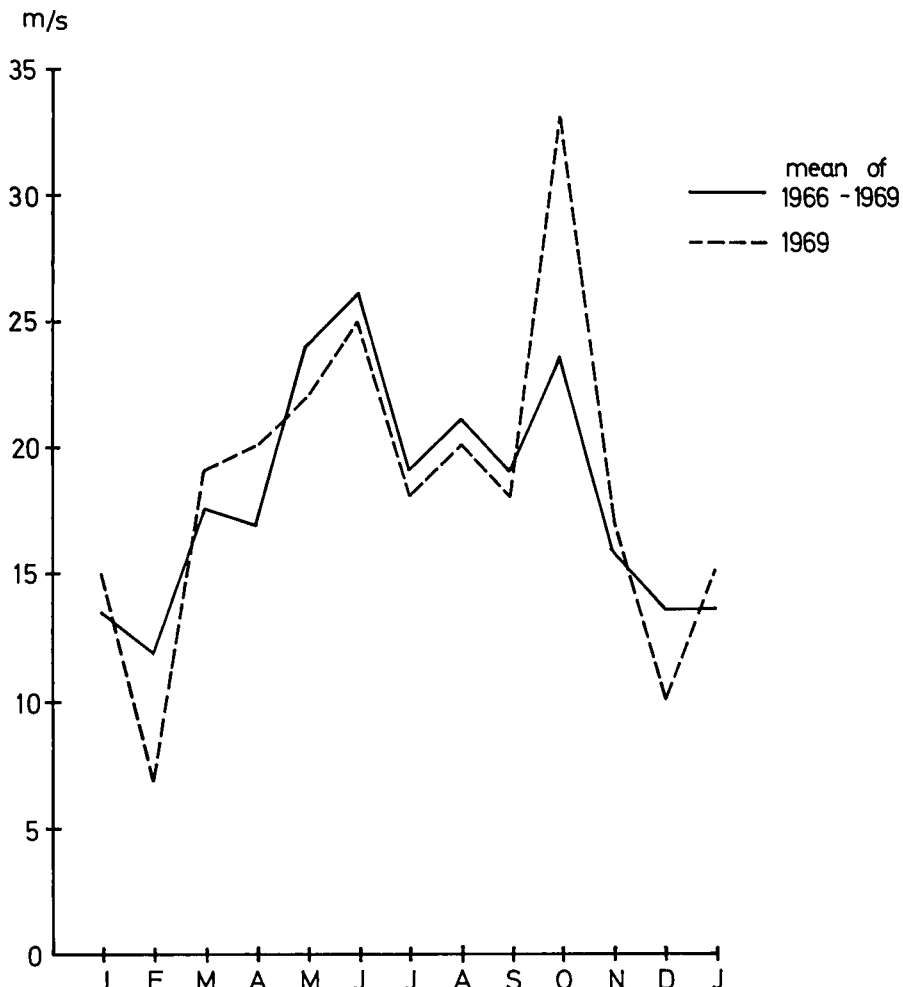


Fig. 2 : Maximum wind velocity at site S.

Average wind velocities during photometric nights

Average wind velocities in m/s were read every two hours from recordings obtained at S and T throughout the year.

Table 3: Frequency of average wind velocity equal to v or less during photometric nights at sites S and T

v m/s	Jan.		Feb.		March		April		May		June	
	S	T	S	T	S	T	S	T	S	T	S	T
1	4	—	32	9	13	10	15	2	1	0	0	0
2	8	—	51	26	25	14	29	6	4	1	2	1
3	10	—	60	36	30	20	40	24	4	4	3	1
4	14	—	65	44	41	26	45	28	7	5	5	2
5	20	—	68	53	43	31	50	38	9	6	7	3
6	25	—	69	57	46	35	54	43	18	7	10	6
7	33	—	61	55	40	58	52	23	10	11	8	
8	39	—	61	68	45	62	61	28	19	13	9	
9	45	—	65	74	50	68	67	36	25	13	13	
10	47	—	65	82	59	74	73	45	33	14	14	
11			69	86	70	75	74	50	40	16	15	
12				88	78	77	76	54	48	19	19	
13				90	86	77	77	54	53	25	23	
14				92	87	77	77	57	55	26	27	
15				94	89	80	77	58	56	30	30	
16				94	91	81	78	58	57	32	31	
17				95	91	82	79	59	60	33	31	
18				95	93	82	82	61	63	35	32	
19				96	93	83	83	66	65		33	
20					94			67	67		35	
21					94			69	69			
22					96			70	70			
v	5.7	—	2.0	4.1	6.4	8.4	5.4	6.8	10.2	11.2	10.6	11.5

Meteorology 1969 on La Silla

Table 3 continued

v m/s	July		Aug.		Sept.		Oct.		Nov.		Dec.	
	S	T	S	T	S	T	S	T	S	T	S	T
1	0	1	12	8	7	4	7	3	5	11	3	29
2	2	4	21	16	14	5	22	13	17	17	18	35
3	9	7	27	22	21	12	32	21	25	22	40	41
4	16	11	34	27	23	17	45	30	31	28	52	50
5	23	15	35	34	26	21	54	41	43	36	59	58
6	28	20	37	34	32	22	60	50	51	43	72	63
7	34	23	44	38	36	26	63	61	64	53	80	74
8	42	36	53	42	38	29	72	66	74	63	88	80
9	55	39	57	49	42	36	75	71	79	67	92	90
10	57	46	67	58	50	42	78	76	82	75	94	92
11	59	54	72	61	57	47		77	85	78		94
12	60	58	75	72	63	50		78	86	82		
13	60	60	80	78	73	55				85		
14	61	61	85	83	76	64				86		
15	63	62	86	86	81	74						
16	64	63	86	87	82	79						
17	64	64	87	87	84	80						
18	66	65	88	89		81						
19		66	89			83						
20						84						
21												
22												
v	7.4	8.6	9.8	10.9	7.9	10.0	4.5	5.3	5.5	6.3	4.6	4.5

B. E. Westerlund

Table 3 gives for sites S and T the number of observations with a wind velocity equal to or less than velocity v as given in the first column.

The last row, indicated by v , gives for each month of the year the average wind velocity at S and T, during photometric nights.

In Fig. 3 the average wind velocities, v , for 1969 and the means of the average wind velocities for 1966—1969 are plotted against the month of the year. The vertical axis gives the average wind velocity in m/s, the horizontal axis gives the month of the year.

The higher velocities occur during the months May to September.

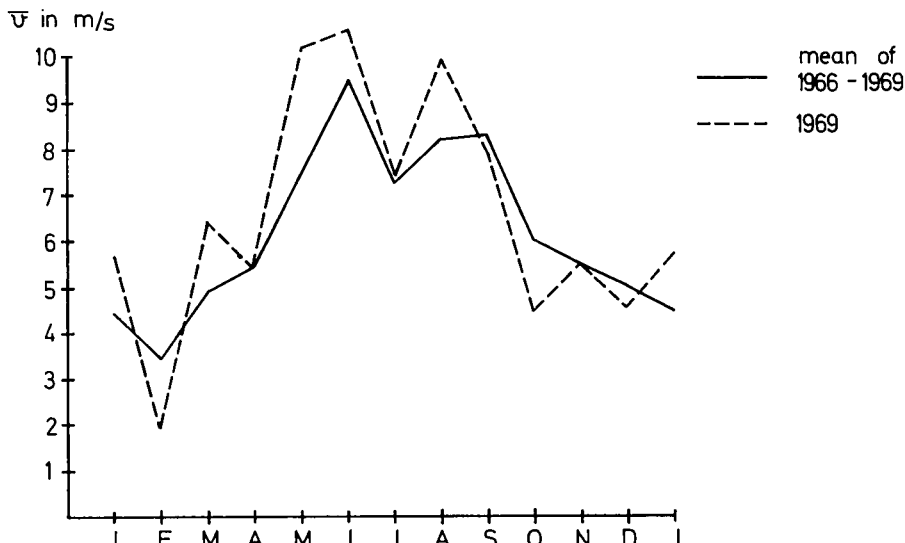


Fig. 3 : Average wind velocity at site S.

Meteorology 1969 on La Silla

Wind directions during photometric nights

At site T only, wind directions were recorded automatically on a wind direction recorder. The records have been read every hour. Table 4 gives for each month of the year the number of hourly observations with a wind direction as indicated in the first column.

This table is based on observations taken during photometric nights only. The last column gives the total results in percentages for 1969. They confirm that the prevailing wind is from NNE during photometric nights, as it was also found in 1967 and 1968.

Table 4: Wind directions at site T during photometric nights

Wind direction	J	F	M	A	M	J	J	A	S	O	N	D	All 1969 in %
S	17	17	3	8	1	0	6	12	9	9	6	18	5.2
SSW	21	21	4	9	2	0	5	61	67	14	9	38	12.3
SW	3	13	8	1	2	0	0	5	3	4	1	5	2.7
WSW	2	1	4	1	0	0	0	1	0	0	0	1	0.5
W	1	0	1	2	0	1	0	6	1	0	2	0	0.7
WNW	0	0	1	0	2	0	0	2	0	1	1	2	0.4
NW	1	4	0	4	0	1	1	4	0	2	1	0	0.9
NNW	0	2	1	8	0	0	0	6	5	5	5	1	1.6
N	16	26	32	33	17	7	18	17	15	20	47	24	13.4
NNE	9	58	133	88	102	56	86	54	52	61	115	79	43.9
NE	14	26	18	8	18	12	18	17	20	25	6	27	10.3
ENE	2	11	3	3	0	0	3	4	4	4	5	12	2.5
E	2	10	1	6	1	0	1	3	2	3	2	8	1.9
ESE	1	0	3	1	0	0	0	1	1	3	1	3	0.7
SE	1	7	2	5	0	0	0	3	1	1	1	7	1.4
SSE	0	2	5	3	1	0	1	4	3	2	5	5	1.5

B. E. Westerlund

The total results in percentage for 1969 are also given in diagram form in Fig. 4. The percentages are plotted against their compass directions.

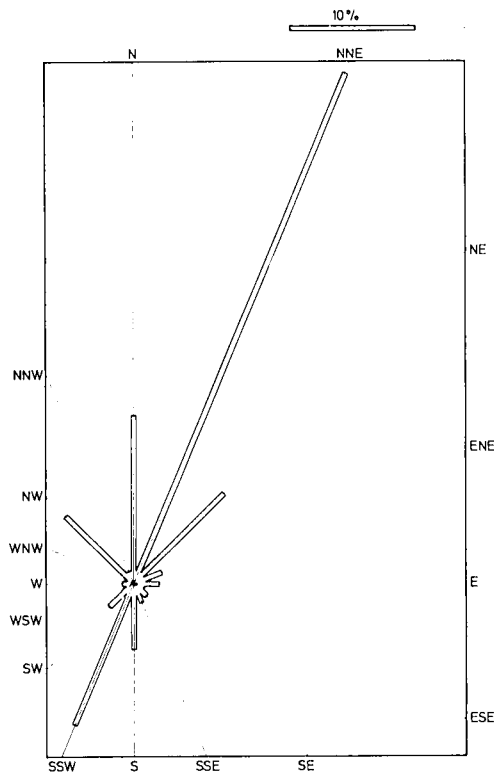


Fig. 4 : Wind directions observed during 1969.

Meteorology 1969 on La Silla

Maximum and minimum temperatures during each month

Table 5 gives for each month the maximum and minimum temperatures as measured at S and T. The temperatures were read daily, regardless of the cloudiness, from a maximum-minimum thermometer.

Table 5

1969		(S)		(T)
	Max. °C	Min. °C	Max. °C	Min. °C
January	+ 23	+ 9	+ 22	+ 11
February	+ 23	+ 9	+ 23	+ 8
March	+ 23	+ 4	+ 23	+ 5
April	+ 24	+ 4	+ 24	+ 5
May	+ 24	+ 3	+ 23	+ 3
June	+ 20	- 7	+ 21	- 7
July	+ 22	- 2	+ 23	- 2
August	+ 22	- 7	+ 22	- 7
September	+ 22	- 1	+ 22	0
October	+ 24	- 2	+ 23	- 2
November	+ 23	0	+ 22	+ 1
December	+ 24	+ 8	+ 24	+ 8

In Fig. 5 maximum and minimum temperatures as measured at S in 1969 and the mean values of 1966—1969 are plotted against the month of the year. On the vertical axis the temperature is given in degrees Celsius, on the horizontal axis the months of the year are indicated.

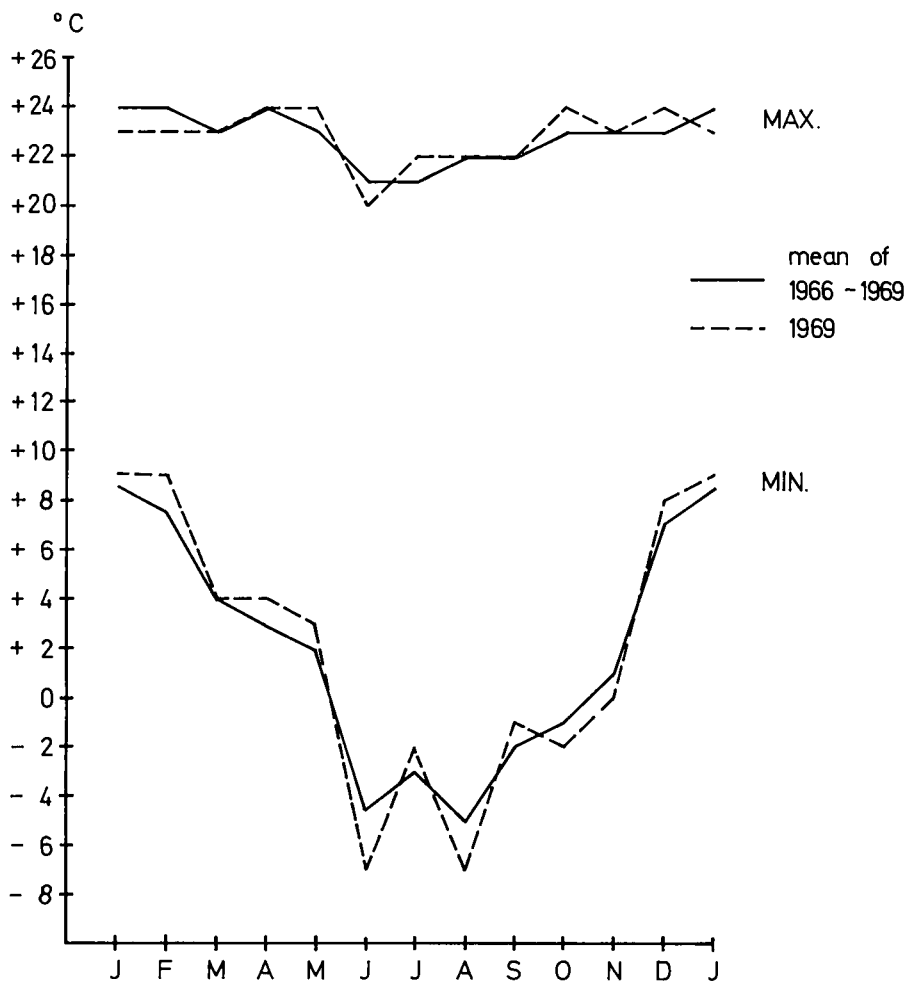


Fig. 5 : Maximum and minimum temperatures at site S.

Meteorology 1969 on La Silla

Table 6: Cumulative table of differences between maximum day temperature and minimum temperature of the following night for the sites S and T

Diff. °C	Jan.		Feb.		March		April		May		June	
	S	T	S	T	S	T	S	T	S	T	S	T
1	0	0	0	0	0	0	0	0	0	0	0	0
2	0	0	0	0	1	0	1	2	0	0	0	0
3	0	0	1	0	1	0	1	3	0	2	1	4
4	1	0	1	0	5	2	1	6	1	3	2	5
5	2	0	1	1	6	2	1	7	2	5	3	7
6	4	1	3	1	9	4	2	8	3	8	6	12
7	7	1	9	4	16	7	7	8	11	12	12	14
8	10	2	15	5	23	11	13	16	16	23	13	16
9	14	2	18	12	28	20	17	23	18	25	17	20
10	17	3	20	14	28	21	24	26	21	27	22	24
11	21		23	14	28	22	27	30	26	29	26	27
12	21		24	16	28	23	28		28	30	27	29
13	21			17	30	25	28		31	31	28	29
14	22						30				28	29
15											30	30
16												
17												
18												
19												
20												

B. E. Westerlund

Table 6 continued

Diff. °C	July		Aug.		Sept.		Oct.		Nov.		Dec.		All 1969 in %
	S	T	S	T	S	T	S	T	S	T	S	T	S
1	0	1	0	0	1	0	0	0	0	0	0	0	1
2	0	1	0	2	1	2	0	0	0	0	0	0	1
3	0	2	0	3	1	3	0	1	0	0	0	0	2
4	1	4	3	6	2	6	0	2	0	1	0	0	4
5	1	4	3	9	3	6	0	4	0	2	0	2	6
6	2	5	5	11	5	8	1	5	0	3	1	3	11
7	3	10	7	11	8	15	3	9	1	6	1	9	24
8	10	17	9	15	15	19	7	15	5	11	2	12	40
9	15	20	12	16	19	23	11	17	14	18	8	16	55
10	20	23	17	18	24	24	18	24	17	24	15	21	71
11	22	26	20	22	26	26	19	25	22	24	18	25	81
12	25	29	25	27	28	29	25	26	25	24	24	25	90
13	27	29	26	29	28	29	26	27	25	25	26	27	93
14	29	30	28	30	29	30	28	28	25	25	27		96
15	29	30	28	30	29		29		27	25			98
16	30	30	30	31	30				27	26			99
17	30	30	30					28					99
18	30	30	31										99
19	30	30											99
20	31	31											100

Meteorology 1969 on La Silla

The differences between the maximum day temperature and the following minimum night temperature have been calculated and are given in Table 6 for all days and nights during the month regardless of the cloudiness. The table gives for each month the number of days for which the temperature difference was equal to or less than the value indicated in the first column.

Due to technical difficulties, the number of days shown in Table 6 is sometimes less than the actual number of days of the corresponding month.

The last column in Table 6 gives for site S the total results in percentage over the year.

Maximum temperature fluctuations during photometric nights

Table 7 gives for each month, for sites S and T, the number of photometric nights during which the maximum temperature fluctuation occurring throughout the astronomical night was equal to or less than the values indicated in the first column.

The astronomical night is defined as the interval of time during which the sun is 18° or more below the observer's horizon.

The last column in Table 7 gives for site S the total results in percentage for 1969.

As in previous years, the observations show the constancy of the temperature during photometric nights.

B. E. Westerlund

Table 7: Cumulative table of maximum temperature fluctuations during photometric nights

ΔT °C	Jan.		Feb.		March		April		May		June	
	S	T	S	T	S	T	S	T	S	T	S	T
1	2	10	4	8	11	15	3	7	1	5	2	4
2	10	15	13	20	15	18	9	12	10	11	4	4
3	14	16	19	21	22	21	13	13	10	12	4	5
4		22			22		13		12		5	5
5		23				15					5	6
6											6	

ΔT °C	July		Aug.		Sept.		Oct.		Nov.		Dec.		All 1969 in %
	S	T	S	T	S	T	S	T	S	T	S	T	S
1	4	2	3	7	3	6	5	8	2	6	5	13	23
2	6	5	12	13	9	10	13	13	14	18	19	22	69
3	8	6	13	15	13	15	14	13	16	20	25	25	88
4	9	8	13	15	16	16		14	20		26	26	96
5		11	15	16									99
6			16										100

Relative humidity during photometric nights

Table 8 gives for sites S and T and each month the percentage of hourly observations for which the relative humidity was equal to or less than the value indicated in the first column. The last column gives the total results in percentage for 1969. The last row, indicated $\bar{R.H.}$, gives for each month of the year the average relative humidity at S and T during photometric nights.

Table 8: Cumulative table of relative humidity at sites S and T

Rel. Hum. %	Jan.		Feb.		March		April		May		June	
	S	T	S	T	S	T	S	T	S	T	S	T
10	0	0	0	0	0	0	0	2	0	0	40	49
20	0	0	3	0	0	1	37	31	26	24	57	59
30	0	5	5	4	8	16	82	79	56	53	89	76
40	3	12	17	14	23	41	98	93	79	65	97	95
50	18	25	50	22	66	79	100	99	89	89	100	96
60	50	52	90	49	89	90		100	92	92		100
70	71	71	100	85	96	96			93	94		
80	85	90		100	99	99			99	95		
90	100	100			100	100			100	96		
100									100			
$\bar{R.H.}$	66	65	53	63	52	48	28	29	37	39	21	23
<hr/>												
Rel. Hum. %	July		Aug.		Sept.		Oct.		Nov.		Dec.	
	S	T	S	T	S	T	S	T	S	T	S	T
10	47	25	45	19	36	33	27	9	3	1	0	0
20	92	80	79	71	40	66	57	46	40	24	0	2
30	100	82	95	78	67	80	78	76	85	54	4	17
40		96	99	91	83	85	90	90	100	88	29	40
50		100	100	97	87	87	98	98		99	75	75
60			100	93	92	99	99		100	94	90	94
70				100	94	99	99			100	97	97
80					96	100	100			100		99
90					97						100	
100					100							
$\bar{R.H.}$	16	22	18	24	27	24	25	28	27	33	49	47
<hr/>												
Rel. Hum. %	All 1969 in % S											
10	16											
20	36											
30	56											
40	68											
50	82											
60	94											
70	97											
80	99											
90												
100												

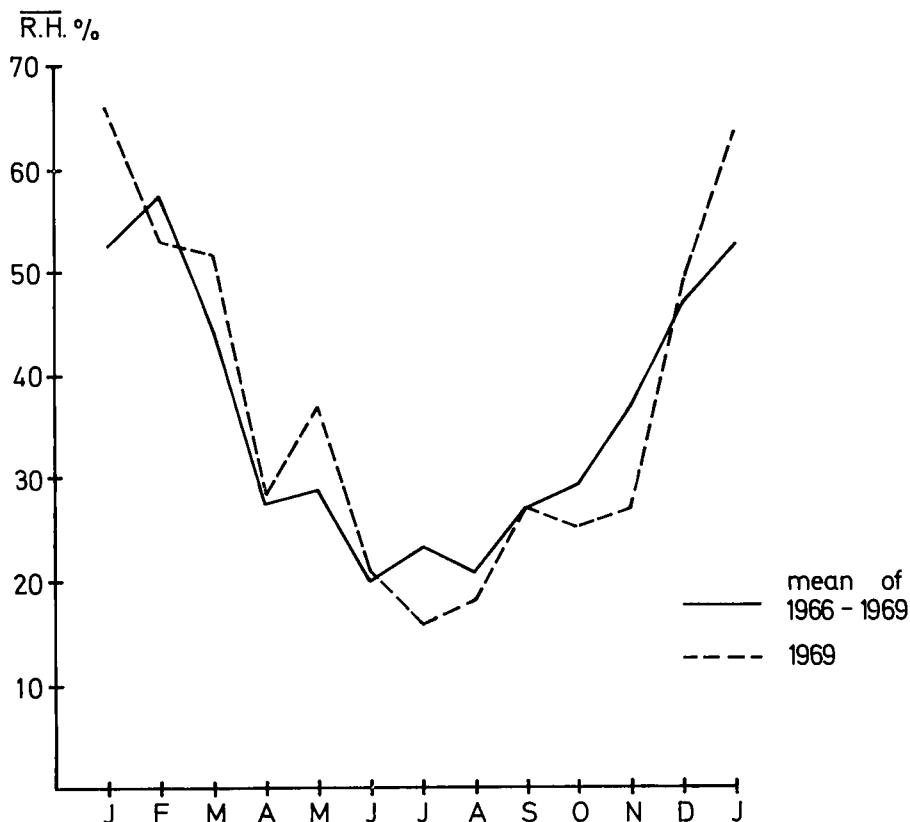


Fig. 6 : Relative humidity at site S.

In Fig. 6 the R.H. at site S is given graphically for 1969 and for the mean of 1966—1969. The vertical axis gives the R.H., and the horizontal axis gives the month of the year.

Prof. Dr. B. E. Westerlund
European Southern Observatory
Casilla 11-P, Correo 9
Santiago de Chile.

SUR LA FLEXION DU GRAND MIROIR DE 3,60 m DE EUROPEAN SOUTHERN OBSERVATORY

G. Lemaitre

I. Paramètres définissant le miroir et le bâillet

La géométrie du miroir est caractérisée par les grandeurs suivantes (voir réf. Texereau) :

Rayon extérieur:	$a = 182,8 \text{ cm}$
Epaisseur au bord:	$t_1 = 53,2 \text{ cm}$
Epaisseur au centre:	$t_0 = 45,5 \text{ cm}$
Rayon intérieur:	$r_0 = 35,0 \text{ cm.}$

Les constantes physiques de la silice fondue constituant le miroir ont pour valeur (voir réf. Corning):

Masse volumique:	$\mu = 2,202 \text{ g} \cdot \text{cm}^{-3}$
Module d'Young:	$E = 0,745 \times 10^6 \text{ kgf} \cdot \text{cm}^{-2}$
Coefficient de Poisson:	$\nu = 0,17.$

Les 33 appuis astatiques dorsaux du bâillet sont disposés comme sur la figure 1:
sur la couronne intérieure de rayon $r_1 = 62 \text{ cm}$: 6 appuis
sur la couronne médiane du rayon $r_2 = 117,5 \text{ cm}$: 12 appuis
sur la couronne extérieure du rayon $r_3 = 170 \text{ cm}$: 12 appuis + 3 appuis fixes.

Les appuis latéraux sont constitués par trois patins fixes et des coussins d'air conformément aux expériences développées récemment par A. Bayle et Ch. Fehrenbach (voir réf.). Les forces exercées par ces coussins sont normales à la tranche du miroir et proportionnelles à la fonction $(1 + \cos\theta)$ ainsi que l'indique la figure 2.

II. Axe du miroir vertical

Si l'on considère la théorie des plaques minces, nous pouvons donner tout d'abord à titres indicatif et comparatif les flèches au centre d'une plaque sans trou appuyée sur ses bords et considérée successivement d'épaisseur constante puis d'épaisseur parabolique. Prenons comme plaque parabolique le miroir non troué.

A masse égale, le calcul donne respectivement $11,8 \mu\text{m}$ pour la plaque d'épaisseur constante et $26,9 \mu\text{m}$ pour la plaque parabolique.

Les hypothèses de départ restant les mêmes, considérons maintenant une plaque d'épaisseur constante de mêmes rayons intérieur r_0 et extérieur a , et de même masse que le miroir.

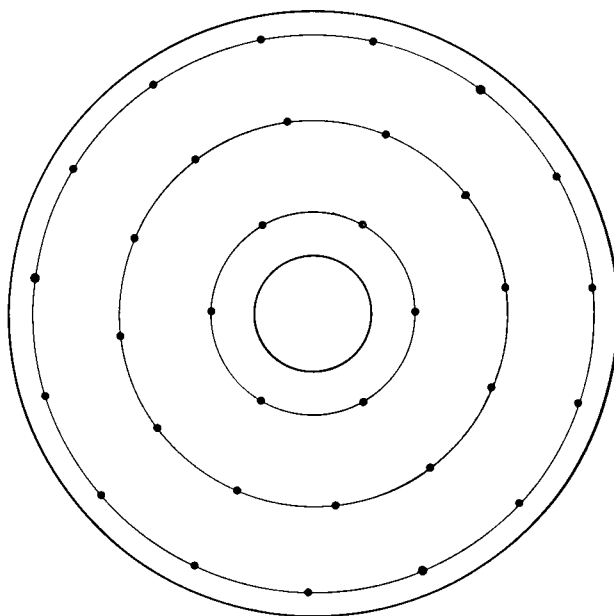


Fig. 1 : Position horizontale. Appuis dorsaux.

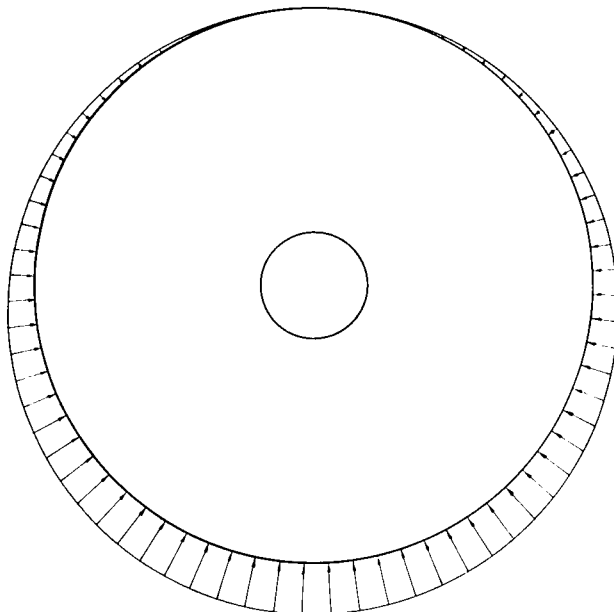


Fig. 2 : Position verticale. Appuis périphériques proportionnels à $[1 + \cos\Theta]$.

Flexion du miroir de 3,60 m

II — 1 : Epaisseur moyenne — masse totale

Si R est le rayon de courbure du miroir, son profil est représenté en 1^{re} approximation par une parabole. L'épaisseur du miroir est alors:

$$h(r) = t_0 + \frac{1}{2R} r^2$$

son épaisseur moyenne est

$$h = \frac{1}{a^2 - r_0^2} \int_{r_0}^a h(r) \cdot 2r dr = t_0 + \frac{1}{2R} (a^2 + r_0^2) = 49,51 \text{ cm.}$$

L'écart maximum à cette épaisseur se situe pour le rayon intérieur r_0 et est égal à 8,1 % de l'épaisseur moyenne.

La masse totale du miroir est égale à 10 970 kg.

II — 2 : Déformation de la plaque d'épaisseur h lorsqu'elle est successivement appuyée sur les trois couronnes d'appui.

Soit $h \mu g$ la force exercée par le champ de la pesanteur sur la plaque mince d'épaisseur constante, rapportée à l'unité d'aire de sa surface, et dirigée suivant la normale. L'équation d'équilibre donnant sa déformation est celle de Lagrange:

$$D \cdot \Delta w(x, y) - h \mu g = 0.$$

Le coefficient D est appelé rigidité de la plaque à la flexion. Considérons tout d'abord que les trois couronnes exercent sur le miroir des forces continues et de révolution. Nous examinerons ultérieurement les effets produits par l'écart à ces hypothèses.

Nous pouvons remarquer dès maintenant que la flèche prise par le miroir lorsqu'il repose sur la couronne médiane devra avoir une influence prépondérante puisque les charges sont dans ce cas les mieux réparties.

Le calcul est fait en variables réduites en prenant successivement dans les trois cas $\varrho = r/r_i$, $i = 1, 2, 3$ et $r_i = \text{rayon d'appui}$.

Le tableau ci-dessous donne les valeurs extrêmes de ϱ .

		rayon intérieur	rayon d'appui	rayon extérieur
$i = 1$	$r =$	35	62	182,8
	$q =$	0,564	1,000	2,950
$i = 2$	$r =$	35	117,5	182,8
	$q =$	0,298	1,000	1,557
$i = 3$	$r =$	35	170	182,8
	$q =$	0,206	1,000	1,075

 q_1 q_2

II — 3 : Répartition des charges

Nous cherchons une répartition des charges exercées simultanément par les trois couronnes d'appui, produisant une déformation minimale. Nous appliquons pour cela le principe de superposition déjà utilisé par A. Couder (voir réf.). Soient $W_1(q)$, $W_2(q)$ et $W_3(q)$ les flèches précédentes et $W_1(q_0)$, $W_2(q_0)$ et $W_3(q_0)$ les valeurs que prennent ces trois flèches pour une certaine valeur q_0 de q . Soient g_1 , g_2 et g_3 les fractions de la charge totale du miroir, exercées par chaque couronne d'appui et telles que l'on ait toujours $g_1 + g_2 + g_3 = 1$. Si l'on désire pour faciliter les comparaisons que la flèche totale W passe constamment par un point fixe d'abscisse q_0 , nous obtenons pour cette dernière :

$$W = \sum_{i=1}^3 g_i [w_i(q) - w_i(q_0)].$$

Les trois fractions qui rendent la flèche totale minimale sont :

$$g_1 = 0,1996$$

$$g_2 = 0,4330$$

$$g_3 = 0,3674$$

ce qui vérifie par ailleurs la remarque que nous avions faite au paragraphe précédent. La figure 4 donne la flèche correspondante ($\Delta w_{\max} = 0,0076$ microns, $\text{pente}_{\max} = 0,0066$ secondes) ainsi que celles situées dans un domaine voisin mais pour une même valeur de g_2 , ceci pour montrer les effets que produisent des écarts de charge inévitables des leviers astatiques. Dans les figures 3 et 5, nous avons considéré également des valeurs différentes de g_2 .

Flexion du miroir de 3,60 m

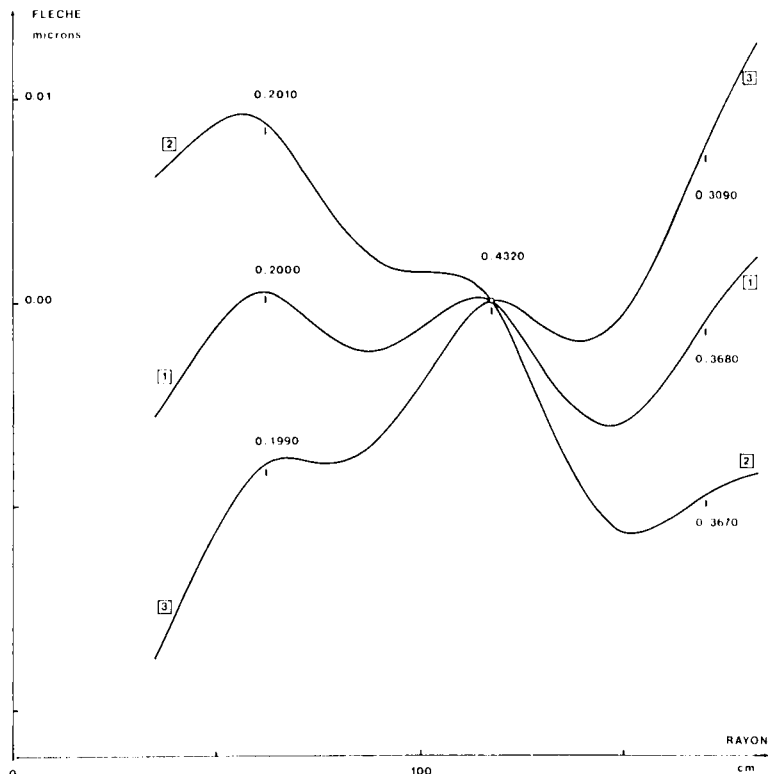


Fig. 3

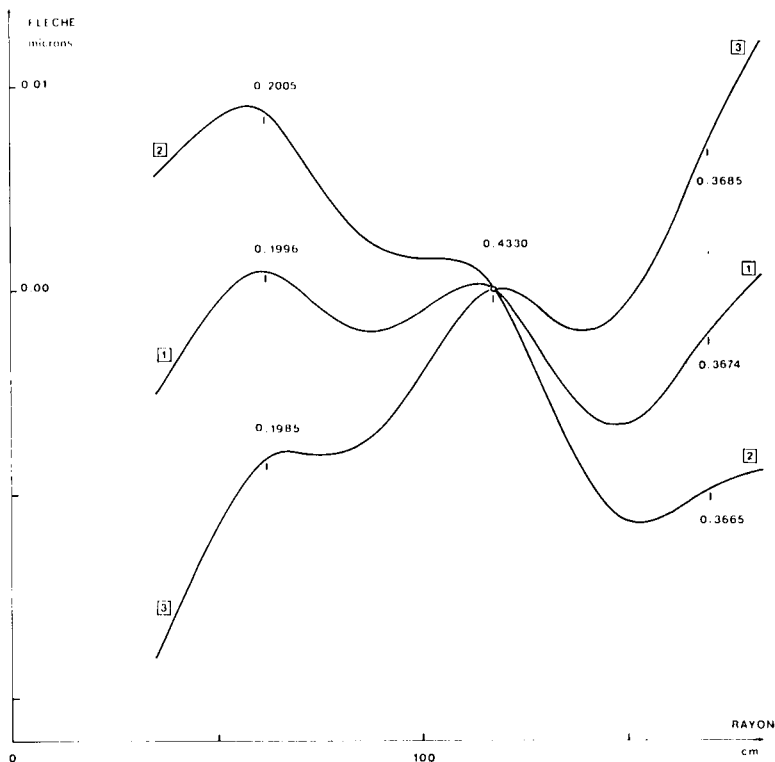


Fig. 4

Flexion du miroir de 3,60 m

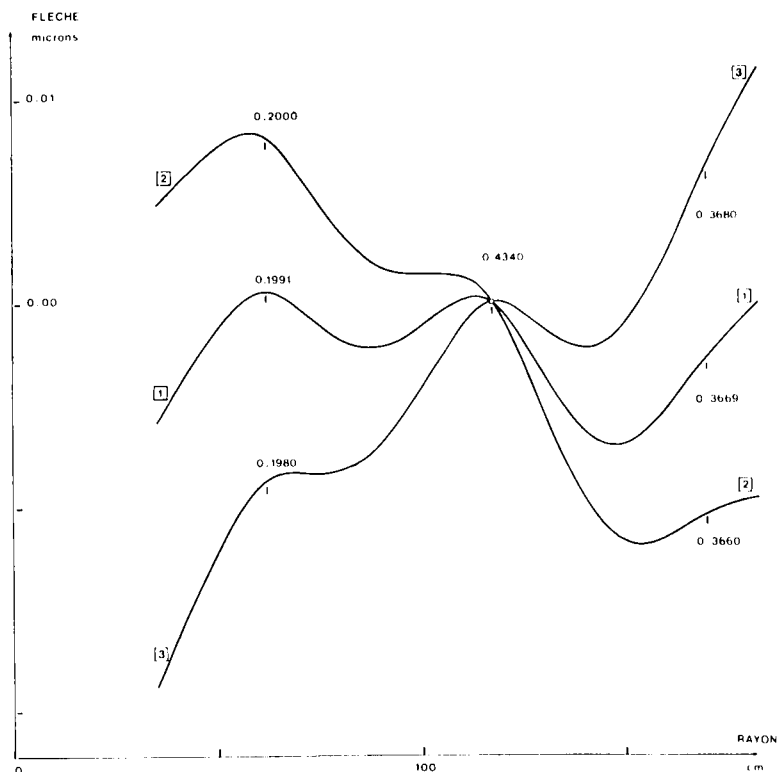


Fig. 5

II — 4 : Epaisseur parabolique

Nous considérons maintenant que la différence d'épaisseur entre la plaque précédente et le miroir produit des effets de flexion indépendants de ceux calculés précédemment. Ceci n'est pas rigoureux mais doit néanmoins donner des résultats plus proches de la réalité puisque l'écart de profil à l'épaisseur moyenne n'est jamais supérieur à 8,1 %.

Le paraboloïde coupe le plan d'épaisseur moyenne suivant une circonférence de rayon égal à $\sqrt{a^2 + r_0^2}/2 = 131,6$ cm. La masse de silice située entre ces surfaces d'un côté ou de l'autre de cette circonférence est :

$$\Delta M = \frac{\pi}{16} \frac{l}{R} (a^2 - r_0^2)^2 = 204 \text{ kg}$$

G. Lemaître

soit une masse relative égale à 0,0186 de la masse totale. Lorsque l'on considère la variation de masse située au droit de la couronne d'appui médiane on comprend que la fraction de charge exercée par cette couronne peut être sensiblement conservée. Nous pourrons donc adopter la répartition suivante :

Couronne intérieure $G_1 = g_1 - 0,0186 = 0,1810$ soit 330,92 kgf par levier astatique

Couronne médiane $G_2 = g_2 = 0,4330$ soit 395,83 kgf — —

Couronne extérieure $G_3 = g_3 + 0,0186 = 0,3860$ soit 282,29 kgf — —

II — 5 : Flexion d'ondulation entre deux points d'appui voisins situés sur une même circonférence d'appui

Ce problème a été étudié par A. Couder (voir réf.) et G. Schwesinger (voir réf.); il apparaît surtout que la déformation est relativement locale et que par voie de conséquence l'énergie contenue dans la partie centrale du disque lorsqu'il est uniformément appuyé sur une couronne se trouve être à peu près conservée si cette couronne d'appui devient discontinue. Dans sa note Schwesinger donne une relation permettant d'évaluer l'amplitude des ondulations W_s . Soit avec nos notations :

$$W_s = c_s \frac{\pi a^4}{E h^2}.$$

Dans le tableau de la page 22 figurent les valeurs de c_s :

S	t_s	r_s	c_s
6	62 cm	0,339	5×10^{-4}
12	117,5 cm	0,643	$2,3 \times 10^{-4}$
15	170 cm	0,932	4×10^{-4}

Les coefficients c_s de la dernière colonne sont des valeurs quadratiques moyennes et doivent être majorées d'un facteur 3,5 à 4. D'autre part il est nécessaire de pondérer ces coefficients en ne considérant que la fraction G_i du poids du miroir.

En prenant $c_s = 5 \times 10^{-4}$ pour valeur majorante de ces trois valeurs et en tenant également compte des flexions de cisaillement, nous obtenons dans les trois cas pris séparément une amplitude de l'ondulation inférieure à $\Delta W_s = 0,015 \mu\text{m}$ pour le miroir partiellement en appui sur une seule couronne.

III. Axe du miroir horizontal

Nous appliquons les résultats obtenus par R. B. Nelson et H. H. Bleich (voir réf.). Dans ces deux mémoires les coefficients figurant dans les tables sont fonction de trois paramètres sans dimension :

$$\varrho_0 := \frac{r_0}{a} = 0,1915$$

$$\beta := \frac{t_0}{a} = 0,2489$$

$$\kappa := \frac{t_1 - t_0}{t_0} = 0,1692.$$

Les pressions $P(\Theta)$ exercées sur la tranche du miroir sont représentées par une série de Fourier, et le coefficient P_n relatif au terme en $\cos n\Theta$ est obtenu de la manière suivante :

$$n = 1 \quad P_1 = 1 + \frac{\kappa}{2} = \varrho_0^2 - \frac{\kappa}{2} \varrho_0^4.$$

Les autres coefficients sont obtenus en considérant la distribution $P(\Theta) = k(l + \cos\Theta)$.

$$n = 0 \quad \frac{P_0}{P_1} = \frac{\int_0^\pi P(\Theta) \cdot d\Theta}{2 \int_0^\pi P(\Theta) \cos\Theta \cdot d\Theta}$$

$$n = 2 \quad \frac{P_2}{P_1} = \frac{\int_0^\pi P(\Theta) \cos 2\Theta \cdot d\Theta}{\int_0^\pi P(\Theta) \cos\Theta \cdot d\Theta}.$$

Dans la répartition considérée figure 2 qui est le cas le plus intéressant étudié par les auteurs nous avons :

$$n : 0 \ 1 \ 2 \ 3 \ 4 \ 5 \ 6$$

$$\frac{P_n}{P_1} : 1 \ 1 \ 0 \ 0 \ 0 \ 0 \ 0.$$

Le calcul nous donne pour $n = 1$, $P_1 = P_0 = 1,048$ et si L est la distance focale du miroir, la flexion est exprimée par

$$(W_s)_{\text{mean}} = \frac{\mu a^5}{100 E t_m^2 L} \left\{ \sum_n |P_n|^2 W_{sn}^2 \right\}^{1/2}.$$

Il nous suffit de connaître W_{s0} et W_{s1} pour obtenir $(W_s)_{\text{mean}}$ puisque les autres coefficients sont nuls dans le cas présent. Les domaines définis par les tables des auteurs nous donnent par extrapolation : $W_{s0} = 0,758$ et $W_{s1} = 0,166$, soit finalement pour le flambage $(W_s)_{\text{mean}} = 0,043 \mu\text{m}$.

IV. Validité des hypothèses — discussion

La silice a été considérée, en premier lieu, comme un corps se déformant élastiquement suivant la loi de Hooke ce qui est rigoureusement exact.

La validité du chapitre II est liée à l'hypothèse d'une plaque mince. Le rapport $h/a = 0,27$ montre bien la nécessité d'apporter ici une correction (voir réf. Timoshenko et Voinowsky-Krieger). Cette correction est due à la distribution des contraintes de cisaillement qui prennent naissance au droit des appuis. Le calcul du miroir aux contraintes de cisaillement sort du cadre de cette étude bien que l'on puisse envisager également une méthode de superposition des charges d'appui. L. A. Selke (voir réf.) a donné les effets produits par ces contraintes pour différentes valeurs du rapport h/a . En référence à cet auteur, il apparaît que dans le cas du présent miroir la majoration à donner à la flexion due aux tensions normales ne devrait pas dépasser 100 %.

Dans la suite de ce calcul il a été ensuite supposé pour obtenir (G_i) que l'écart au profil d'épaisseur parabolique produisait des effets de flexion indépendants de la flexion générale. D'autre part, pour la répartition (G_i) la variation de la rigidité engendre approximativement une augmentation d'amplitude de 20 % au niveau du rayon intérieur, qui diminue lorsqu'on s'éloigne du centre, s'annule vers $r = 131,6$ cm et se traduit finalement par une diminution d'amplitude de 15 % au niveau du rayon extérieur. Compte tenu également de la flexion d'ondulation, la flexion totale du grand miroir lorsque son axe est vertical ne dépasse pas 0,040 μm et se situe plutôt vers 0,030 μm .

Dans le chapitre III, la déformation de 0,043 μm par flambage est du même ordre de grandeur. Le miroir étant constitué d'une juxtaposition d'hexagones de silice refondue, nous dirons pour conclure que les effets d'anisotropie sont bien difficiles à prévoir. Enfin, il faudra obtenir dans la réalisation et la mesure des forces concernant chaque levier astatique une précision du 1/1000 qui seule permettra d'obtenir les déformations minimales.

Conclusion

Bien qu'une autre répartition de la géométrie des appuis permettrait de gagner un facteur 2 sur la déformation et sur la pente, l'optimisation sur les charges d'appui semble être suffisante pour conclure que le bâillet défini précédemment remplira correctement ses fonctions.

La déformation qu'il engendre par flambage ne dépasse pas 0,043 micron et une pente maximale de 0,052 seconde. Lorsque l'axe du miroir est au zénith l'optimisation de la flexion donne une flèche maximum de 0,040 micron, une pente maximum de 0,110 seconde et correspond à la répartition suivante de la masse totale :

Flexion du miroir de 3,60 m

0,1810 pour la couronne intérieure
0,4330 pour la couronne médiane
0,3860 pour la couronne extérieure

soit en considérant une masse totale de 10 970 kg pour le miroir, une distribution respective de 330,9 ; 395,8 ; et 282,3 kgf pour chaque levier astatique.

REFERENCES

- A. Bayle et
Ch. Fehrenbach 1967, Recherche expérimentale d'un barillet anti-flexion pour un grand miroir astronomique. ESO Bulletin No. 2, 41.
- Corning Glass Works 1966, Corning fused silica code 7940. N. Y.
March 1.
- A. Couder 1931, Déformation des grands miroirs. Bull.
astr. 7, 262 et 267.
- R. B. Nelson and
H. H. Bleich 1968, Tables for deformation of the optical
effects of gravity on radially supported
telescopic mirrors. Columbia University,
New York. July.
- G. Schwesinger 1966, General characteristics of elastic mirror
flexure in theory and applications. Symposium
on support and testing of large astronomical
mirrors. Tucson (Arizona), p. 20,
21 and 22.
- L. A. Selke
— 1970, Appl. Opt. 9, No. 1, January.
Appl. Opt. 9, No. 6, June.
- J. Texereau 1969, Examen du disque de 365,6 cm pour l'ESO
après réfection de la couche supérieure.
Usine Corning de Canton, N. Y., le 13
juin.
- S. Timoshenko et
S. Voinowsky-Krieger 1961, Théorie des plaques et coques. P. 72.

Dr. G. Lemaître
Observatoire de Marseille
2, Place Le Verrier
13 Marseille 4^e, France

OBSERVING PROGRAMS FOR EARLY TYPE STARS WITH EXTENDED ATMOSPHERES *)

Anne B. Underhill

When choosing an observing program for astrophysical purposes, one must start out with a quantitative description of the spectrum and determine the changes, if any, with time of the spectrum as well as just what is present. By comparing observed line profiles and equivalent widths with those predicted using the best available physical theory, one should be able by an iterative process to obtain insight about the temperature and pressure structure in a stellar atmosphere, its change with time and the abundances of the elements. These conclusions should, in principle, permit one to deduce something about the evolution of stars and the rate at which observable changes in stellar spectra occur. Conclusions regarding particular stars can be generalized to conclusions significant for the evolution of a galaxy by demonstrating that the stars studied are representative of groups of stars in the galaxy.

The types of quantitative information needed are (i) wavelengths and identifications (many rather strong absorption lines and a considerable number of emission lines are still unidentified in early type spectra), (ii) the equivalent widths of lines, particularly of those lines important for the analysis of stellar atmospheres, and (iii) line profiles. An enormous amount of work of this sort could be done. In order to maximize the amount of scientific information obtained in comparison to the amount of observing and reduction work which is done, it is important to select carefully the stars and the spectral details to be studied. This means thinking seriously about the meaning of the methods of analysis which are used and whether the available spectroscopic equipment can yield the needed observed facts.

The following remarks concern programs which would be profitable and interesting to do using the coudé spectrograph of the 152 cm telescope. Other problems of great interest arise concerning stars of later type but these topics will not be mentioned. The early type stars with extended atmospheres can be divided into three classes:

- Extreme cases — shell stars and Wolf-Rayet stars
- Moderate cases — supergiants of types A 2 to O 9
- Border-line cases — some main-sequence stars.

* Paper presented at the ESO Colloquium, Nice 3-5, 1969.

Shell stars

Among well known shell stars having negative declinations one has 17 Leporis and 48 Librae. Undoubtedly other bright shell stars exist in the southern hemisphere. Further intensive observation is desirable for the above stars in order to supplement and extend the long series of observations which already exist. It is most valuable to be able to relate observations made from the southern hemisphere with those made from the north in order to control instrumental problems and to make sure no systematic differences occur.

With shell stars the highest dispersion is needed in order to obtain line profiles, and the wavelength coverage should be from 3100 Å to at least 6700 Å. Some observations in the photographic infrared region would also be very useful. By continuing the documentation on radial velocity, line strengths and line shapes, one will be amassing a body of material that will serve as a basis for any theory of how the outer atmosphere of a star may change and of which spectral details are sensitive indices of what sort of physical process.

It is important with shell stars to have a homogeneous set of spectrograms of the best possible spectral purity covering a long time range (20 years or more). Only then can one hope to relate the development in time of the spectrum with the actual physical conditions in the extended atmosphere. A program such as this is now far more attractive than ever before because of our increasing theoretical knowledge of how to handle the problem of spectrum formation when the restrictive hypothesis of LTE is not made.

The observed spectrum is a blend of the spectrum of the underlying star and that of the shell. Some observations of the spectra of similar stars, but without shells, should be made with the same spectrograph in order to furnish spectrophotometric data which may be subtracted from the composite spectrum of the star plus shell in order to reveal precisely how strong the shell lines are and what are their shapes. It is particularly necessary to have information about the H and He I line profiles in "normal stars", in order to find reasonably precisely the shapes of the hydrogen and He I lines formed in the shell.

Wolf-Rayet stars

The brightest Wolf-Rayet stars are in the southern hemisphere. Some such as γ_2 Velorum and Θ Muscae are spectroscopic binaries, thus one has a blended spectrum. Nevertheless, owing to their apparent brightness, observation of the southern Wolf-Rayet stars is the best way in which to augment significantly our meager quantitative knowledge about line strengths and shapes in Wolf-Rayet stars. In the case of binary stars one must observe around the orbit in order to separate the Wolf-Rayet spectrum satisfactorily from that of the companion. In addition a few lines in Wolf-Rayet spectra (chiefly those which are formed in a gas stream between the components or in an envelope of gas surrounding the two stars) are known to vary irregularly in rather short intervals of time.

Early Type Stars with Extended Atmospheres

No satisfactory picture of what is occurring can possibly be deduced without a thorough coverage over several revolutions in the binary orbit. Such a program would take up a lot of observing time; its practical value must be assessed against the background of knowledge acquired from the study of shell spectra and the spectra of supergiants. There is no doubt that any series of spectra of the brighter Wolf-Rayet stars will show many details, some of which will be variable. The theoretical side of the problem is the one which appears least clear at the moment. However, significant theoretical advances probably cannot take place without the stimulus given by a set of homogeneous spectrophotometric data obtained over a considerable period of time.

Supergiants

The early type supergiants have very distinctive spectra and form a rather homogeneous group so far as visual absolute magnitude is concerned because M_V lies between about —6 and —7. Their spectral types run from A 2 to O 9. The luminosity classes are I a and I b usually, with a few stars being assigned the intermediate luminosity class I ab. Although any experienced spectrum classifier can place the stars rather consistently in one or other of the luminosity classes, only a few isolated pieces of information exist about the quantitative differences in spectrum between classes I a, I ab and I b. It is of interest to find out quantitatively what these differences are and to interpret these differences in terms of differences in atmospheric structure and possibly evolutionary stage.

Since the early type supergiants are among the intrinsically brightest stars, it is the spectra of such stars that will be most easily observed in external galaxies such as the Magellanic Clouds. Soundly based deductions about the significance of the presence or absence of such stars in any external galaxy or cluster can only be made after an unambiguous understanding has been obtained about the implications of supergiant spectra concerning the stage of evolution of stars, their masses and their composition. It is not difficult to show that conditions are such in the atmospheres of supergiants that the spectra must be interpreted without making the hypothesis of LTE. This means that progress will be made most unambiguously by studying line profiles as well as equivalent widths.

The absorption lines of early type supergiants are naturally rather broad, typically with a total width at half intensity of 0.5 to 1.0 Å. Although only moderate spectral purity can usually be used with stellar spectrograms, the projected slit width being of the order of 0.2 to 0.3 Å, it is possible to obtain true line profiles of lines in the spectra of the apparently bright early type supergiants. Thus the early type supergiants form an attractive group of objects for detailed spectrophotometric study.

Already it is known that several interpretational problems exist. For instance, the Balmer and Paschen series break off near $n = 23$, which according to the Teller-Inglis formula suggests that the electron density in the atmosphere is

between 10^{12} and 10^{13} . Such a density is not incompatible with the shapes of the He I lines, some of which appear to show weak Stark broadened components (this point requires more study in order to demonstrate what is precisely the case) nor with the rather large general opacity which is needed to give the large photosphere implied by the value of M_V . However, LTE model atmosphere calculations based on a standard H:He composition imply at such electron densities rather larger Stark wings for the H lines than are observed and deeper cores. Allowance for non-LTE would tend to make the cores even deeper, cf. what happens with shell stars, but it would not change the wings much. A promising way to resolve this conflict is to postulate that the atmospheres of the supergiants of luminosity class I a are hydrogen poor, perhaps by a factor 10. What the case is for the supergiants of luminosity of class I b is at present unknown.

Although the conflict between LTE theory (with qualitative non-LTE improvements) for the hydrogen lines can be diminished by accepting an electron density of the order of 10^{11} , the conflict between the predictions for other lines and the observed line strengths and shapes cannot be reconciled. The other lines in supergiants are generally very much wider and stronger than can be predicted using classical model atmosphere theory for stationary plane parallel layers. If one looks only at equivalent widths, some sort of a match between theory and observation can be obtained by introducing a large value for the arbitrary parameter "microturbulence". However, the physical significance of this procedure is far from clear and it is desirable to develop sounder physical theories which can be controlled by comparing observed and calculated line shapes as well as equivalent widths.

In the case of main-sequence stars a fairly satisfactory understanding of the meaning of spectral type, at least as applied to the shape of the continuous spectrum, is beginning to emerge. However, in the case of the supergiants it is by no means clear that the trend of spectral types from A 2 to O 9 corresponds to a uniformly increasing effective temperature. Spectral types are assigned usually from several empirically selected ratios of line strengths. However, the spectral types which result are bunched at certain types. This is shown by the histogram of Figure 1 which gives the distribution with spectral type of supergiants of types A 2 to O 9 having southerly declinations. The data were taken from the **Bright Star Catalogue**, Third Edition. The luminosity classes I a, I ab and I b are taken together.

There are 53 supergiants of types A 2 to O 9 with southerly declinations and apparent magnitudes brighter than 6.6 mag. Thirty-two of these are class I a, 11 class I ab, and 10 class I b. It is seen that 23 are classified as type B 1 or earlier, 7 as B 3, 6 as A0 and 5 as A 2. The remaining twelve are scattered at other types. It would be interesting to find out the meaning of the fact that such a large percentage of the brighter southerly supergiants have types between B 1 and O 9. Bias factors due to the distribution of interstellar absorption and to the shape of our galaxy must be taken into account before attributing much significance to this apparent distribution of the supergiants over the spectral types.

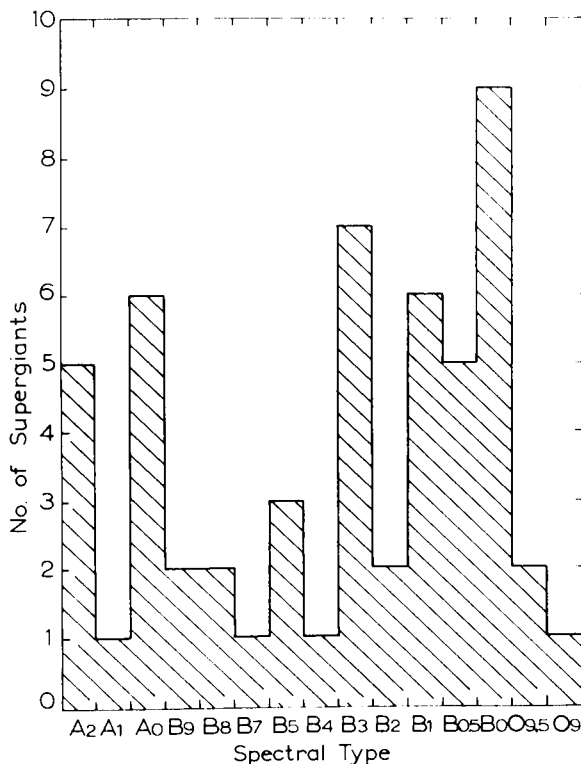


Fig. 1 : A histogram of the supergiants of types A 2 to O 9 having negative declinations with magnitudes brighter than 6.6. Luminosity classes Ia, Iab and Ib are taken together.

Main-sequence stars

Among the main-sequence stars with southern declinations one has stars of all sorts and many interesting binary systems. The problems of spectrum interpretation raised by peculiar stars such as 3 Centauri A and α Sculptoris are part of the general problem introduced by the existence of Bp and Ap stars. In a nutshell, it appears that stars which have closely the same continuous spectrum and hydrogen-line spectrum may have quite a different line spectrum when the weak lines are examined. About ten per cent of the late B and early A type stars fall into the class "peculiar". Very many of the lines which appear to be anomalously strong or anomalously weak with respect to their relative strengths in the so-called normal stars are particularly sensitive to the physics of the line-formation process. Consequently it is not certain that the apparent

variations in line strength should be interpreted directly as evidence for abundance anomalies. This problem requires further detailed study using an adequate theory of line formation and testing the results of theory by comparing line profiles as well as equivalent widths. However, very little information about line profiles in main-sequence B type stars exists, particularly for the peculiar stars. In many cases the peculiar stars have very sharp lines and the spectral purity of the available spectrograms is inadequate to yield meaningful true profiles. The problem of obtaining profiles for stars with very sharp lines can probably best be solved by observing a few carefully selected lines in some carefully selected stars by interferometric methods.

A related problem is the evaluation of the rapid change of line-shape and intensity which has been detected in a few stars near the main-sequence, particularly those of the β Canis Majoris class of variables and the O 9 V standard star, 10 Lacertae. Further information about these line-shape changes and their behaviour in time is essential if a better understanding of the meaning of the spectra of main-sequence stars is to be obtained. An observing program designed to gather the needed information requires very short exposures and high spectral purity, thus use of an image tube is indicated.

The helium stars form a class of extreme objects in which the hydrogen lines have negligible strength and the He I and other lines are strong. Three of them have negative declinations and the other two known objects can be reached from the southern observatories. More information is needed about these objects, but it is a difficult observational problem because all of the known objects are faint. One star, HD 125823, is known in which the He I lines vary in strength. This southern object (declination $-39^\circ 3'$, V = 4.41) deserves further study. An adequate set of line profiles and equivalent widths used with properly developed non-LTE theory would help to show how sensitive the strengths and profiles of the He I lines are to the physical conditions in the stellar atmosphere. Once this problem has been solved, it will be possible to conclude with some confidence what the true meaning of "helium-weak" and "helium-strong" spectra is.

Prof. Dr. Anne B. Underhill
Astronomical Institute
Utrecht, The Netherlands

ADDRESSES

- | | |
|-------------------------------|--|
| ESO Directorate | 131 Bergedorfer Straße, 205 Hamburg 80,
Fed. Rep. of Germany. Telephone: 7 21 30 01.
Telex: 2 17 856. Telegrams: EURASTRO Hamburg. |
| ESO TP Division | (Telescope Project Division),
Ch 1211 Genève 23, Switzerland.
Telephone: (022) 41 98 11. Telex: 23 698.
Telegrams: CERNLAB — Genève. |
| ESO Headquarters
Chile | Alonso de Córdova 3107, Vitacura. Casilla 11 P
— Correo 9, Santiago de Chile.
Telephone: 28 50 06. Telex: 3520048.
Telegrams: ESOSER — Santiago de Chile. |
| ESO Guesthouse | Gustavo Adolfo 4634, Santiago de Chile.
Telephone: 48 42 54
(near cross-roads Avenida Cristóbal Colón and
Amerigo Vespuicio, then through Félix de Amesti). |
| ESO Local Office
La Serena | Casilla 27 D. Balmaceda 595, La Serena, Chile.
Telephone: 11 67, 11 77. Telegrams: ESOSER —
La Serena |

The ESO Observatory on La Silla can best be reached by mail, telegrams etc. via Santiago Headquarters (address see above).

